Advances in Radiation Oncology (2025) **10**, 101764

advances in radiation oncology

www.advancesradonc.org

Scientific Article

Targeting Active Microglia Alleviates Distal Edge of Proton Radiation-induced Neural Damage

Keman Liao, PhD,[a,b,c,1] Dan Ou, PhD,[a,b,c,1] Mei Chen, PhD,[a,b,c,1] Fei Xu, MD,[a,b,c,1] Jianyi Zhao, BS,[a,b,c] Li Zhou, BS,[a,b,c] Ran Wu, PhD,[a,b,c] Yingying Lin, PhD,[a,b,c,*] Yibin Zhang, BS,[a,b,c,*] Lu Cao, PhD,[a,b,c,*] and Jiayi Chen, PhD[a,b,c,*]

[a]*Department of Radiation Oncology, Ruijin Hospital, Shanghai Jiaotong University School of Medicine, Shanghai, China;* [b]*Shanghai Key Laboratory of Proton-Therapy, Shanghai, China; and* [c]*Institute for Medical Imaging Technology, Shanghai, China*

Received 15 October 2024; accepted 9 March 2025

Purpose: Proton therapy (PT) has distinct advantages in its ability to precisely target tumors while avoiding adjacent normal tissues. However, the distal edge effects of PT constrain its application. This study investigated the brain tissue response in the distal edge regions of protons and compared it with the effect of photons.

Methods and Materials: The occurrence of damage from photons and at the distal edge of protons was investigated in a murine model. Bragg peak treatment plans for murine models were optimized. Hematoxylin and eosin and immunofluorescence staining were performed along the distal margin. In addition, the approximate distance from the Bragg peak to the neuronal damage sites was calculated. Furthermore, a small-molecule inhibitor was studied for its ability to inhibit microglia activation.

Results: The distal edge brain injury murine model was successfully established. Reactive gliosis and granulovacuolar neuronal degeneration were observed in the right hemisphere of the brain in the proton irradiation group. Neuronal injuries were observed at multiple locations (the frontal lobe, thalamus, and cerebral cortex) along the distal border, but no injured neurons were detected along vertical photon irradiation exposed areas. Meanwhile, severe neural damage was seen with horizontal photon irradiation. At the distal edge of the Bragg peak (0.4633 ± 0.01856 cm), microglia with abnormal morphology accumulated. IBA1 and CD68 staining revealed activated microglia at the corresponding neuronal damage sites, indicating their involvement in irradiation-induced damage. Activated microglia were not observed with vertical photon irradiation, whereas many activated microglia were observed with horizontal photon irradiation. Moreover, asparagine endopeptidase inhibitors administered via intraperitoneal injection significantly reduced active microglia in the thalamus and cerebral cortex and alleviated brain damage.

Conclusions: This study demonstrated that proton radiation induces neuronal damage and accumulation of activated microglia at the distal edge. Targeting activated microglia may play a protective role in distal edge injury from radiation.

Sources of support: This work was supported by the National Key R&D Program of China (grant number 2023ZD0502206), National Natural Science Foundation of China (grant numbers 82373514, 81772654, 82273278, 82002630), the Shanghai Association for Science and Technology (grant number 201409003000), Shanghai Science and Technology Innovation Action Plan (grant number 23Y41900100), the National Key Research and Development Program of China (grant number 2022YFC2404602), Shanghai Hospital Development Center Foundation (grant number SHDC12023108), Scientific and Technological Innovation Action Plan of Shanghai Science and Technology Committee (grant number 22Y31900103), Beijing Science and Technology Innovation Medical Development Foundation (grant number KC2021-JX-0170-9), and China Postdoctoral Science Foundation (grant number 2024M752028).

All data generated and analyzed during this study are included in this published article (and its supplementary information files).

[1]K.L., D.O., M.C., and F.X. contributed equally to this work.

*Corresponding authors: Jiayi Chen; Email: cjy11756@rjh.com.cn; Lu Cao; Email: cl11879@rjh.com.cn; Yibing Zhang; Email: zyb40472@rjh.com.cn; and Yingying Lin; Email: yylin@sibs.ac.cn

https://doi.org/10.1016/j.adro.2025.101764

Introduction

Unlike radiographs, proton therapy (PT) has the radiophysical benefit of the "Bragg peak" (BP), which allows for rapid dose reduction beyond the target and precise irradiation. Currently, the number of PT centers worldwide has expanded almost exponentially.[1] Therapeutic indications have also been extended to tumors in pediatric cases, brain tumors, breast cancer, and other malignancies.[2-5] Although most studies assessing PT support its ability to reduce toxic side effects, the effects of the distal edge of proton radiation on organs at risk constrain its broader application.

In patients with low-grade glioma, PT-induced contrast-enhanced lesions were exclusively observed at the distal edge of the proton beam.[6] Another PT center reported increased radiosensitivity within the periventricular zone, identifying a spatial correlation between radiation-induced brain injury (RIBI) and increased relative biological effectiveness (RBE).[7] An increase in rib fracture rate was observed in the MOSAIQ (Elekta AB, Stockholm, Sweden) database, attributed to the distal edge effects of PT.[8] These reports emphasize the critical need to investigate the biological mechanism of distal edge effects to ensure safer PT application.

Microglia can adapt to any form in the central nervous system, but an imbalance in their homeostasis, along with uncontrolled activity, can cause persistent and irreversible damage.[9] Activated microglia produce high levels of proinflammatory cytokines, including tumor necrosis factor, interleukin (IL) 1β, and IL-6, which can induce neuronal injury, death, and oxidative stress. The presence of activated microglia also reduces levels of neuroprotective factors, further exacerbating neuronal damage.[10] After ischemia, microglial phagocytosis of excitatory synapses contributes to synapse loss in the penumbra and leads to long-term neurologic impairment.[11] Anticoagulants, bevacizumab, α-tocopherol, pregabalin, and hyperbaric oxygen have been used in clinical trials. However, the unclear mechanisms of microglia activity impede the development and application of clinical protective medicine.

Asparagine endopeptidase (AEP) is a potential target for RIBI and is a cysteine proteinase in the C13 family of peptidases.[12] AEP is elevated and activated in brain injury or degenerative diseases, such as Alzheimer disease, and cleaves key components, such as tau and amyloid precursor protein.[13,14] Moreover, we previously found that AEP targets microglia to induce neuronal senescence, a critical aspect of its role in RIBI.[12] Many AEP-specific activated precursor drugs (coupled with doxorubicin) and AEP small-molecule targeted inhibitors (membrane-penetrating and nonpenetrating) are used in intervention therapy.[15] These findings motivated us to reduce RIBI using AEP inhibitors (AEPIs).

In this work, we established single-proton-beam and photon beam treatment murine RIBI models. We compared the morphologic changes and performed staining of brain slices along the irradiated and distal edge regions, 2 hours postirradiation. Neuronal damage and microglial activation were induced using photons or distal edge proton irradiation. Furthermore, targeting activated microglia may play a protective role in distal edge injury during PT.

Methods and Materials

Animals and radiation therapy

Twenty-four male C57BL/6 mice, aged 7 to 8 weeks, were purchased from Lingchang Biotech. Mice were randomly assigned to different irradiation groups and irradiated with 10 Gy photons or protons. According to the biologically effective dose equation, a single dose of 10 Gy is equivalent to a clinically relevant dose.

Irradiation treatments were performed at Shanghai Key Laboratory of Proton Therapy. For photon therapy, the left hemisphere of the brain of 6 mice was photon irradiated using a 6-MV radiograph beam at 10 Gy/1 Fx and a dose rate of 300 cGy/min. For vertical irradiation with an radiograph beam directed from top to bottom, the Gantry was set at 0°, whereas for horizontal irradiation directed from left to right, the Gantry was set at 270°. For both irradiations, the source-surface distance was set to 100 cm with 0.5 cm of solid water for dose building, and a radiation field of 1 × 1 cm was used. Mice were fixed in a prone position after anesthesia, and the left hemisphere was marked with white tape (on the top or on the side). The light field and laser line were used to assist with mouse positioning (Figs. 1 and E1).

Irradiation was conducted using a medical linear accelerator (Varian Trilogy). For PT, a single-proton beam was directed on the left hemisphere using a fixed horizontal proton beam line for irradiation. A dose of 10 Gy (RBE 1.1) was administered. Using the linear-quadratic model[16] to predict the total radiation delivered to the tissue when doses are administered in fractions, and employing an α/β ratio of 3 for late effects in normal brain tissue, an acute exposure of 10 Gy is approximately equivalent to a total dose of 26 Gy administered in repeated 2 Gy fractions in a clinical setting. The 10 Gy dose selection was in line with previous reports.[17] An 85.3 MeV pencil beam scanned the BP using a RayStation treatment planning system. Mice were placed in a prone position under total anesthesia. The radiograph alignment of their jaw was adjusted to match the irradiation plan (Fig. 1). Detailed steps are listed in the Supplementary Materials.

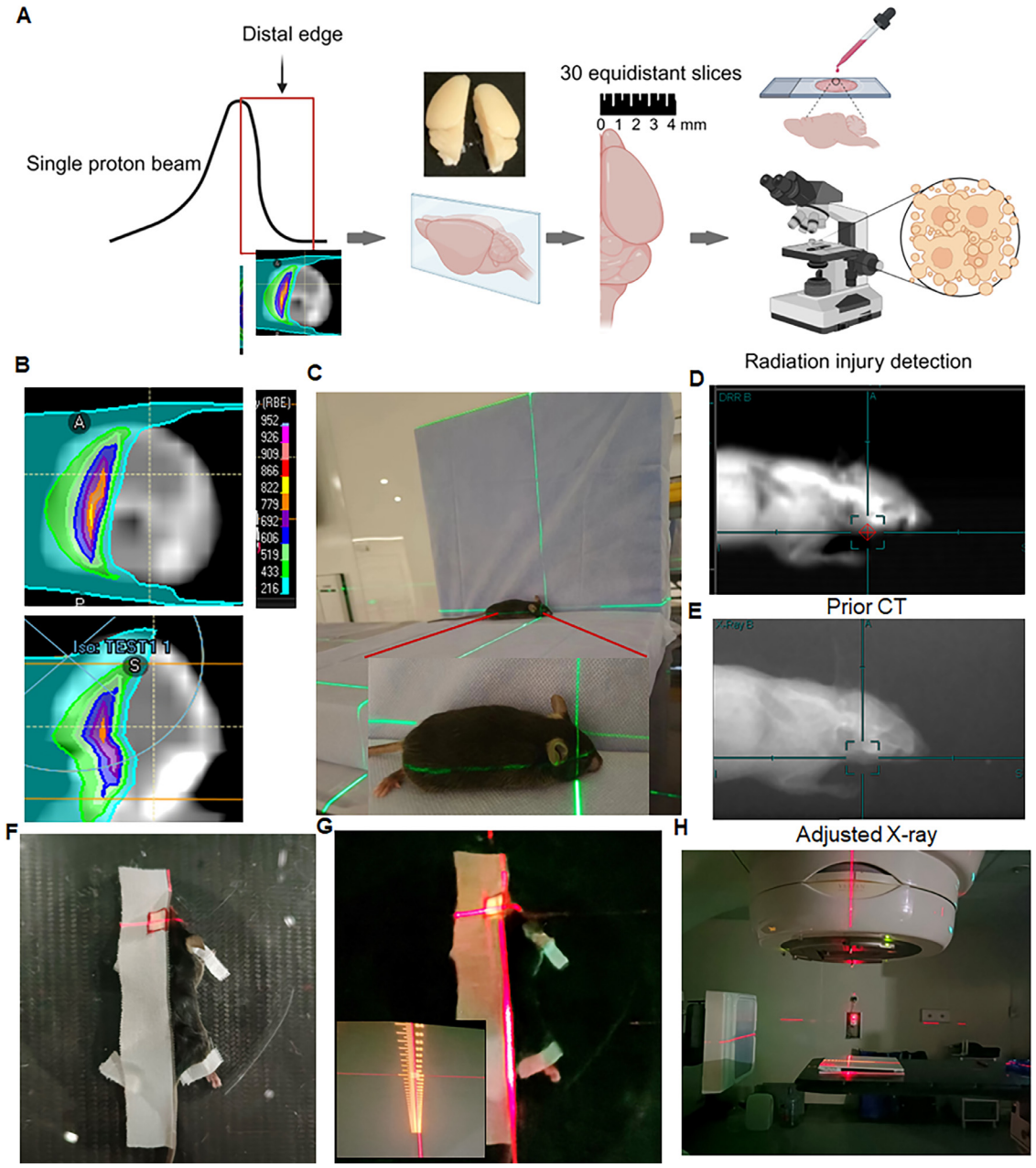

Figure 1 Schematic diagram and construction of the distal edge injury of the Bragg peak in the murine radiation-induced brain injury model. (A) Schematic illustration of the model. (B) Beam arrangement used for irradiation in mice. (C) Position of mice under laser guidance during proton therapy. (D, E) Radiograph alignment during irradiation. (F) Position of mice under laser guidance during photon therapy. (G) The left hemisphere was marked with white tape with a radiation field of 1 × 1 cm; source-surface distance was set to 100 cm with 0.5 cm of solid water for dose building during photon therapy. (H) The Gantry was set to 0° for vertical irradiation.

Hematoxylin and eosin staining

Hematoxylin and eosin (H&E) staining was performed on paraffin-embedded sections for 5 minutes, followed by a wash with running water and a 3-minute eosin counterstain. Sections were sealed after staining, and the slide scanning system SQS-40P (TEKSQRAY) was used for imaging.

Administration of AEPI

An aqueous solution of AEPI (HY-114174; MCE) was purchased. Six male C57BL/6 mice were intraperitoneally administered with phosphate-buffered saline (G4202; Servicebio) or 10 mg/kg AEPI. The mice were anesthetized for irradiation 2 hours later.

Section preparation and immunofluorescence staining

Tissues were fixed in paraformaldehyde 2 hours after radiation and sectioned at a thickness of 3 to 5 μm onto glass slides. The primary antibodies used for immunofluorescence staining are listed in the Supplementary Materials.

Statistics

Statistical analyses were performed using the SPSS 21.0 (IBM Corporation). Data were analyzed using 2-tailed Student *t* tests, 1-way analyses of variance, Pearson's correlation analyses, Kaplan−Meier analyses, and log-rank tests. A statistically significant result was defined as

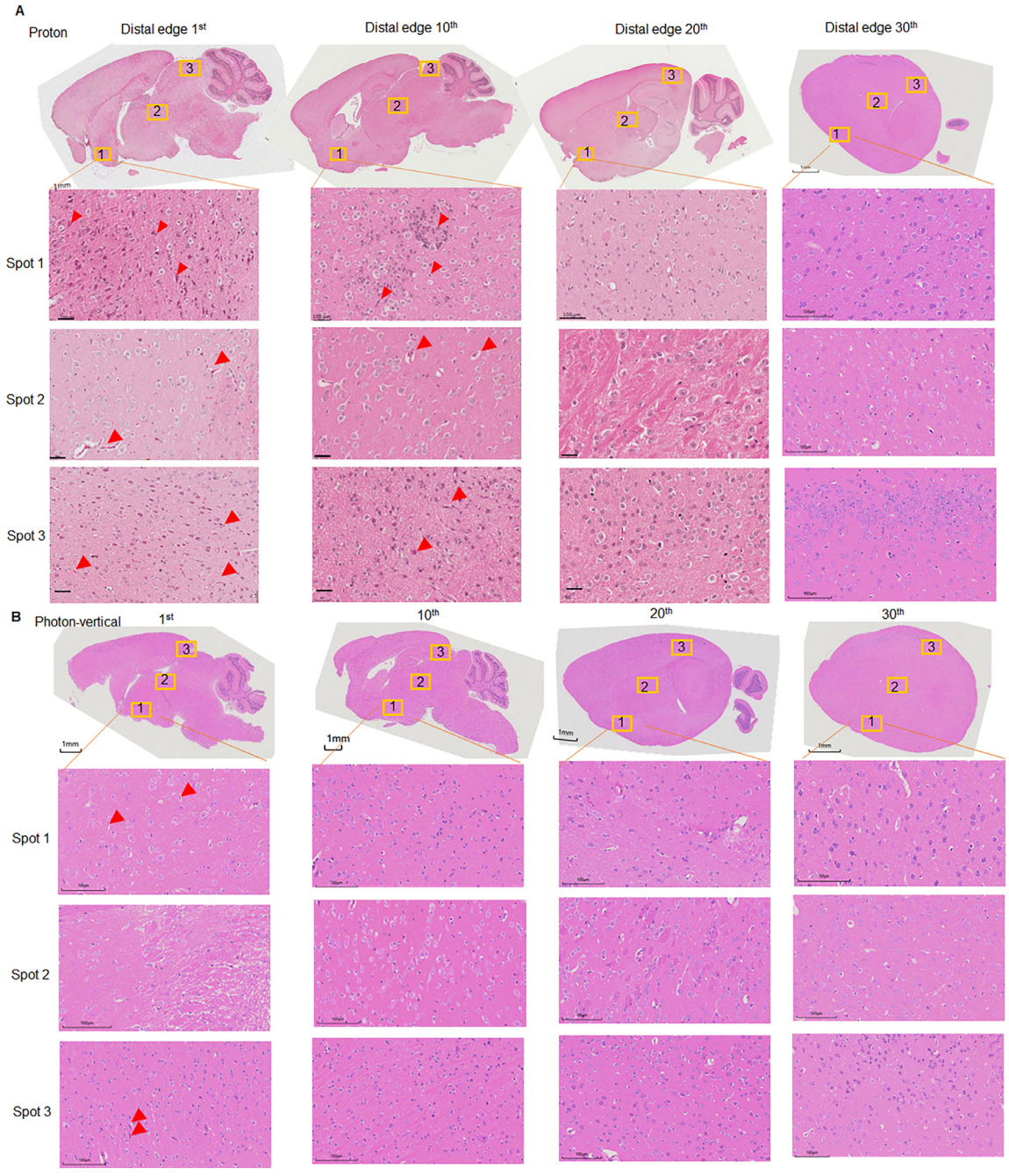

Figure 2 Hematoxylin and eosin (H&E) staining of different sites in the right hemisphere of the irradiated model. (A) H&E staining of necrotic cells, granulovacuolar neuronal degeneration, reactive gliosis, and irregular microglia in different sites of proton-irradiated slices. Red arrow indicates abnormal cell morphology. Scale bars: 1000 μm for the sagittal view, 50 μm for the 1st, 10th, and 20th slices, and 100 μm for the 30th slice. (B) H&E staining of necrotic cells in different sites of vertical photon-irradiated slices. Red arrowheads indicate abnormal cell morphology. Scale bars: 1000 μm for the sagittal view and 100 μm for the enlarged view.

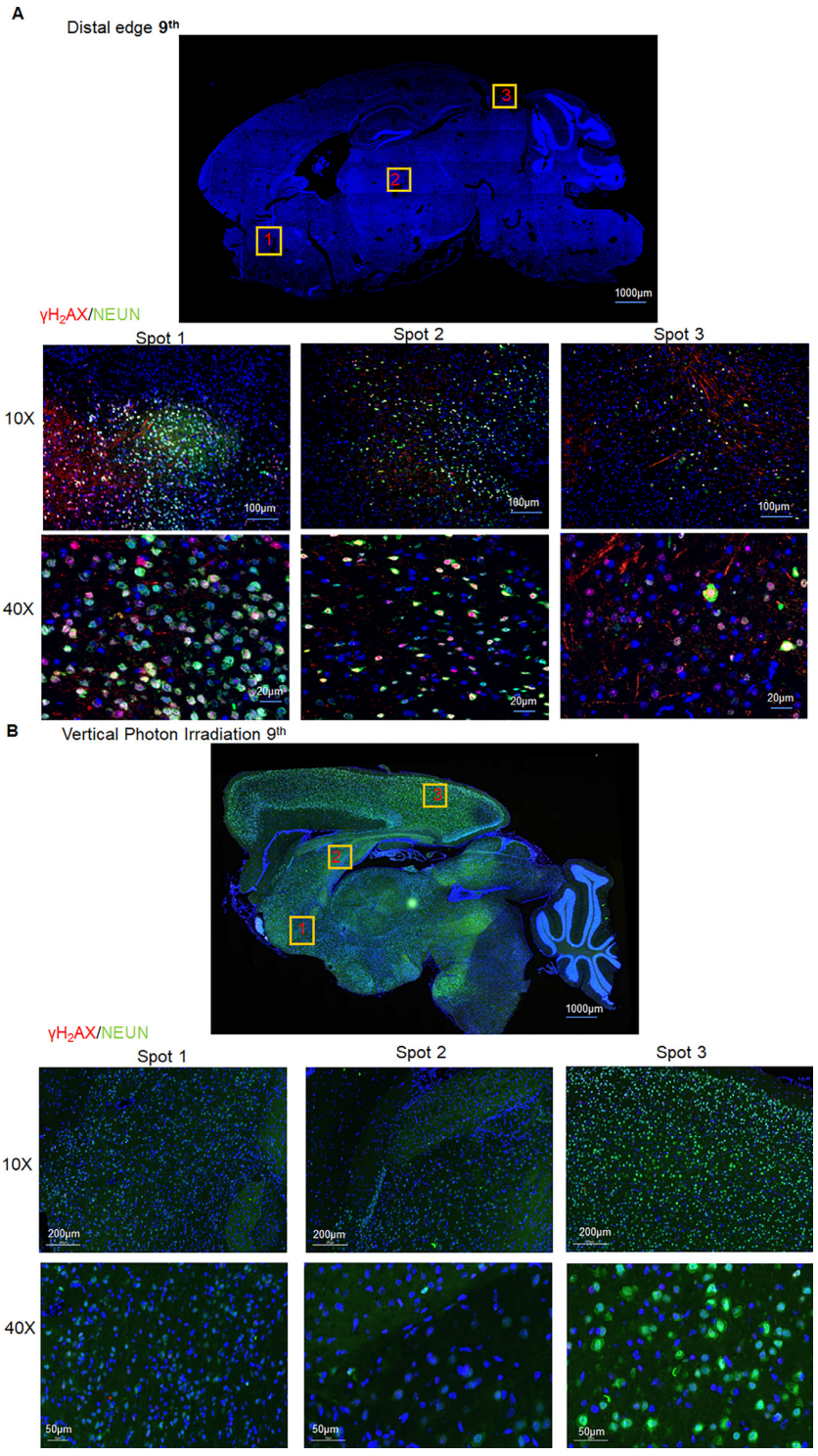

Figure 3 DNA damage and neuron damage observed in the 9th slice using immunofluorescence assay. (A) Representative fluorescence images of γ-H_2AX/NeuN immunostaining in different regions of brain slices of mice exposed to proton irradiation. Scale bar: 1000 μm for the sagittal view, 100 μm for 10 $\times$, and 20 μm for 40 $\times$. Nuclei are stained with DAPI (4',6-diamidino-2-phenylindole) (blue). (B) Representative fluorescence images of γ-H_2AX/NeuN immunostaining in different regions of brain slice of mice exposed to vertical photon irradiation. Scale bars: 1000 μm for the sagittal view, 200 μm for 10 $\times$, and 50 μm for 40 $\times$. Nuclei are stained with DAPI (4',6-diamidino-2-phenylindole) (blue).

having a 2-tailed *P* value <.05. GraphPad Prism 7 (GraphPad Software Inc) was used for graphic representations.

Results

Construction of the murine RIBI model

Because the irradiation location of the mouse brain is stable and less affected by respiratory movement, we established a brain irradiation model to study terminal injury (Fig. 1A). Following clinical protocols, radiation plans were developed and executed, with routine optimization using the computed tomography (CT) scan (Fig. 1B-E). A single 10 Gy RBE proton beam was targeted to the left hemisphere, positioning the BP in the left hemisphere and its distal edge (the low-dose region) in the right hemisphere.

Two-photon beam angles were used for photon irradiation. For the radiograph beam directed from top to bottom, lead blocking reduced the lateral penumbra to simulate the rapid drop of the proton distal edge

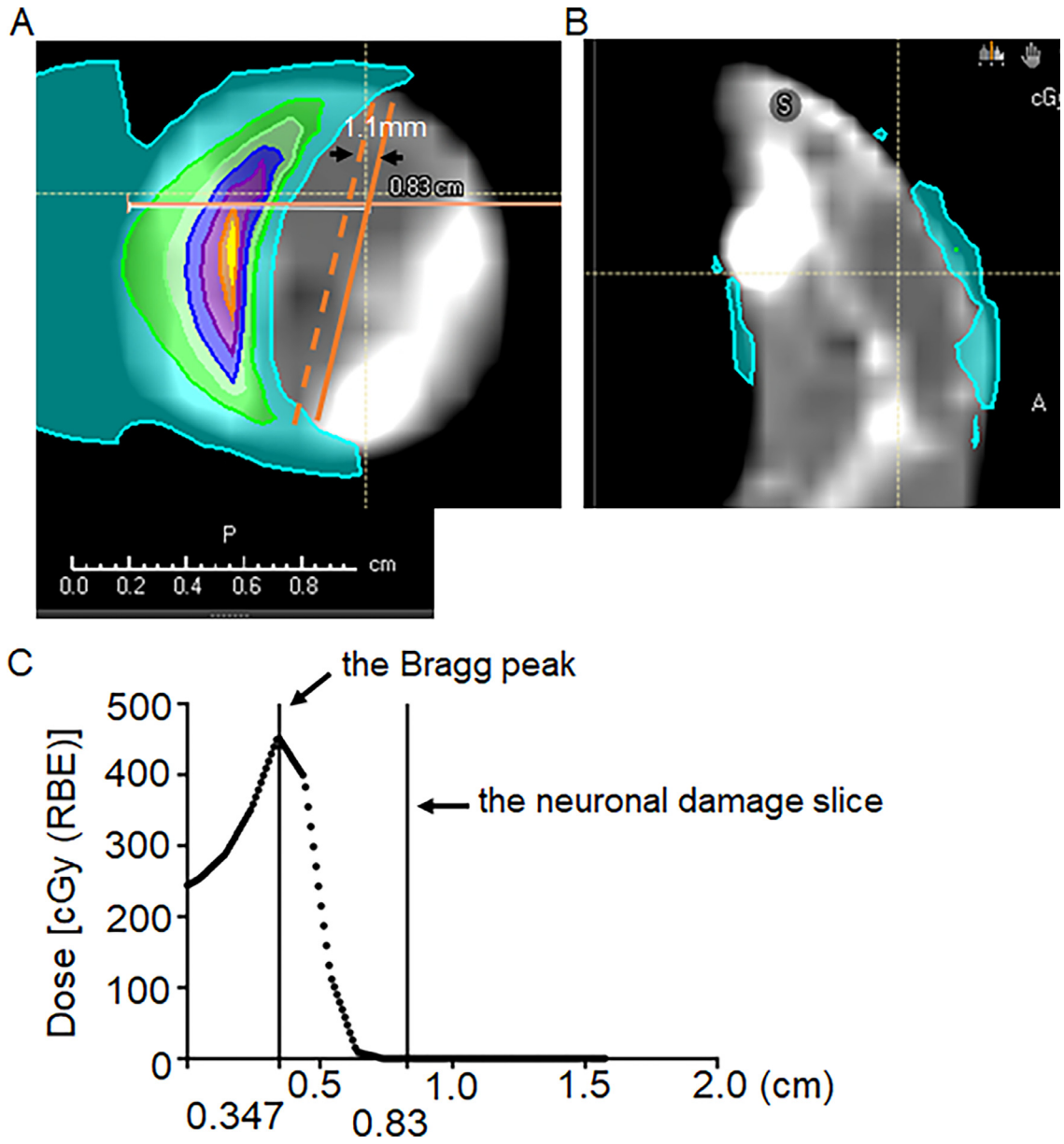

Figure 4 Neuronal damage in relation to isodose lines in different sections. (A, B) Representative images of the slices with neuronal damage and isodose lines in axial and sagittal views. The dotted line represents the midline of the brain. The solid line indicates where neuronal damage was detected. The sagittal section corresponds to the region with detected neuronal damage. (C) Dose distribution with penetration depth. The Bragg peak position and slice with neuronal damage are marked on the curve.
Abbreviation: RBE = relative biological effectiveness.

(Fig. 1F-H). For horizontal photon irradiation directed from left to right, we used the same angle as in the proton irradiation model to study terminal photon injury. The light field and laser line were used to assist mouse positioning (Fig. E1A-D).

The irradiated brains were extracted, preserved, and embedded in paraffin, and the right hemisphere was equally divided into 30 slices for examination.

Neural damage is present at the distal edge of the BP in vivo

Pathological changes such as necrotic cells and inflammatory cell infiltration were identified using H&E staining. Reactive gliosis and granulovacuolar neuronal degeneration were observed in the frontal lobe of the first slice, which is the BP area. No major damage was observed in the 30th slice. The 10th and 20th slices were also evaluated for biological damage. The 10th slice displayed diffuse injury at multiple locations in the frontal lobe, thalamus, and cerebral cortex, which is the distal edge of the BP or low-dose area. H&E staining revealed basophilic necrotic neurons, reactive gliosis, and clusters of small, round cells (Fig. 2A). In the photon irradiation models, the 1st, 10th, 20th, and 30th slices of the right hemisphere revealed no major damage in the vertical irradiation group (Fig. 2B). However, in the horizontal irradiation group, the 20th slice revealed multiple small, round cells, and the 30th slice displayed basophilic necrotic neurons (Fig. E2).

NeuN was used to measure neuronal density, and γ-H2AX was used to assess DNA damage in the 9th slice through immunofluorescence. Coimmunostaining of NeuN with γ-H2AX revealed neurons with DNA damage 2 hours after irradiation, indicating extensive neural damage at the distal edge of the BP in our model (Fig. 3A). However, the 9th slice from the vertical photon irradiation group did not show noticeable red fluorescence, indicating that DNA damage was not detectable by γ-H2AX staining (Fig. 3B). In contrast, mice treated with horizontal photon irradiation exhibited prominent orange fluorescence, indicative of substantial neuronal DNA damage (Fig. E3). We further mapped neuronal damage at the distal locations relative to the isodose lines on CT scans (Fig. 4). The average distance from the detected neuronal damage slices to the median sagittal surface of the brain was 2.007 $\pm$ 0.4648 mm (n = 6). The approximate maximum distance from the BP to the farthest reported point of neuronal damage on the axial section was 0.4633 $\pm$ 0.01856 cm (n = 6) (Table 1).

These findings demonstrate that neuronal damage occurred at multiple sites at the distal edge of the proton BP in vivo, whereas injured neurons were not observed along the vertical photon irradiation side. Moreover, neural damage was severe under horizontal photon irradiation.

Table 1 Average distance of detected neuronal damage slices from the median sagittal surface of the brain and the Bragg peak of protons

Sample	Distance to median sagittal surface of brain (mm)	Distance to Bragg peak (cm, on axial section)
1	1.1	0.48
2	0.9	0.47
3	4.03	0.38
4	2.34	0.51
5	1.95	0.49
6	1.82	0.45
Average $\pm$ SD	2.007 $\pm$ 0.4648	0.4633 $\pm$ 0.01856

Distal damage mediated by activated microglia is reversed with AEPI administration during PT

We examined the surface markers IBA1 and CD68 of the small, round cells, which resembled microglia, found in the 10th slice. Notably, the corresponding neuronal damage sites (frontal lobe, thalamus, and cerebral cortex) showed a larger number of microglia, as evidenced by IBA1 and CD68 staining (Fig. 5A). This suggests that the nonlinear radiation damage described above could be because of secondary injury mediated by activated microglia. However, the 11th slice of the vertical photon irradiation group revealed minimal microglial activation, based on IBA1 and CD68 staining (Fig. 5B). In contrast, mice administered with horizontal photon irradiation exhibited more orange fluorescence in the 11th slice, indicating microglial activation (Fig. E4).

Next, we explored the role of AEPI, a protective agent for RIBI, during proton irradiation. After irradiation, significant microglial activation was observed in the thalamus and cerebral cortex (Fig. 6A-D). γ-H2AX staining revealed clearly detectable fluorescence signals in the proton group, and AEPI significantly reduced γ-H2AX immunofluorescence signals in cells irradiated with either proton or photon irradiation (Fig. 7A-D). These results suggest that AEPI effectively protects DNA from radiation.

Discussion

Recently published data on radiation necrosis at the distal edge of the BP over time in PT suggest that unfavorable outcomes cannot be disregarded.[18] A more conservative brainstem dose limit using protons is now employed

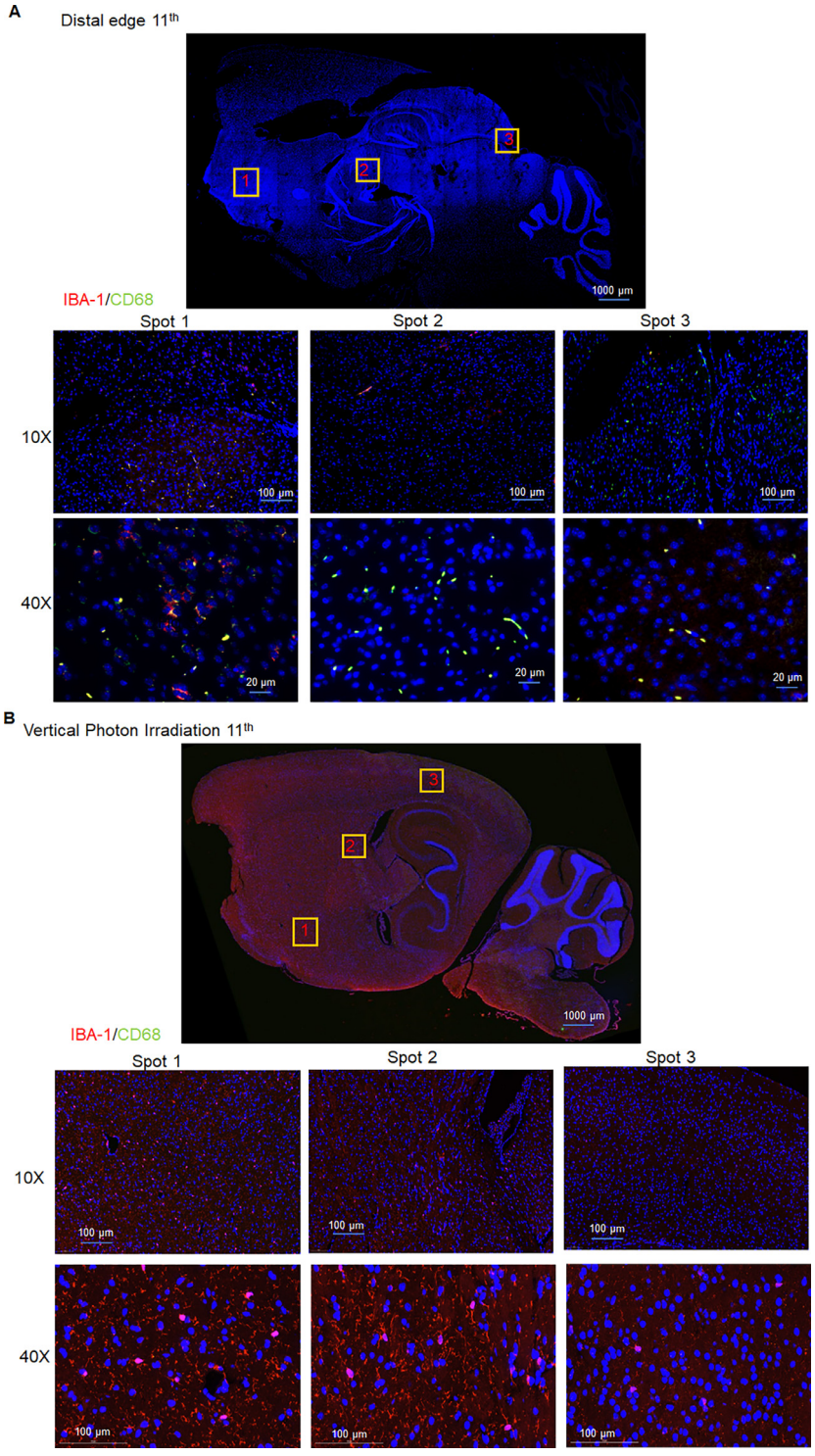

Figure 5 Microglia activation observed in the 11th slice using immunofluorescence assay in the irradiated model. (A) Representative fluorescence images of IBA1/CD68 immunostaining in slices from different regions of the brain of mice exposed to proton irradiation. Scale bars: 1000 μm for the sagittal view, 100 μm for 10 ×, and 20 μm for 40 ×. Nuclei are stained with DAPI (blue). (B) Representative fluorescence images of IBA1/CD68 immunostaining in slices from different regions of the brain of mice exposed to vertical photon irradiation. Scale bars: 1000 μm for the sagittal view, 100 μm for 10 ×, and 100 μm for 40 ×. Nuclei are stained with DAPI (blue).

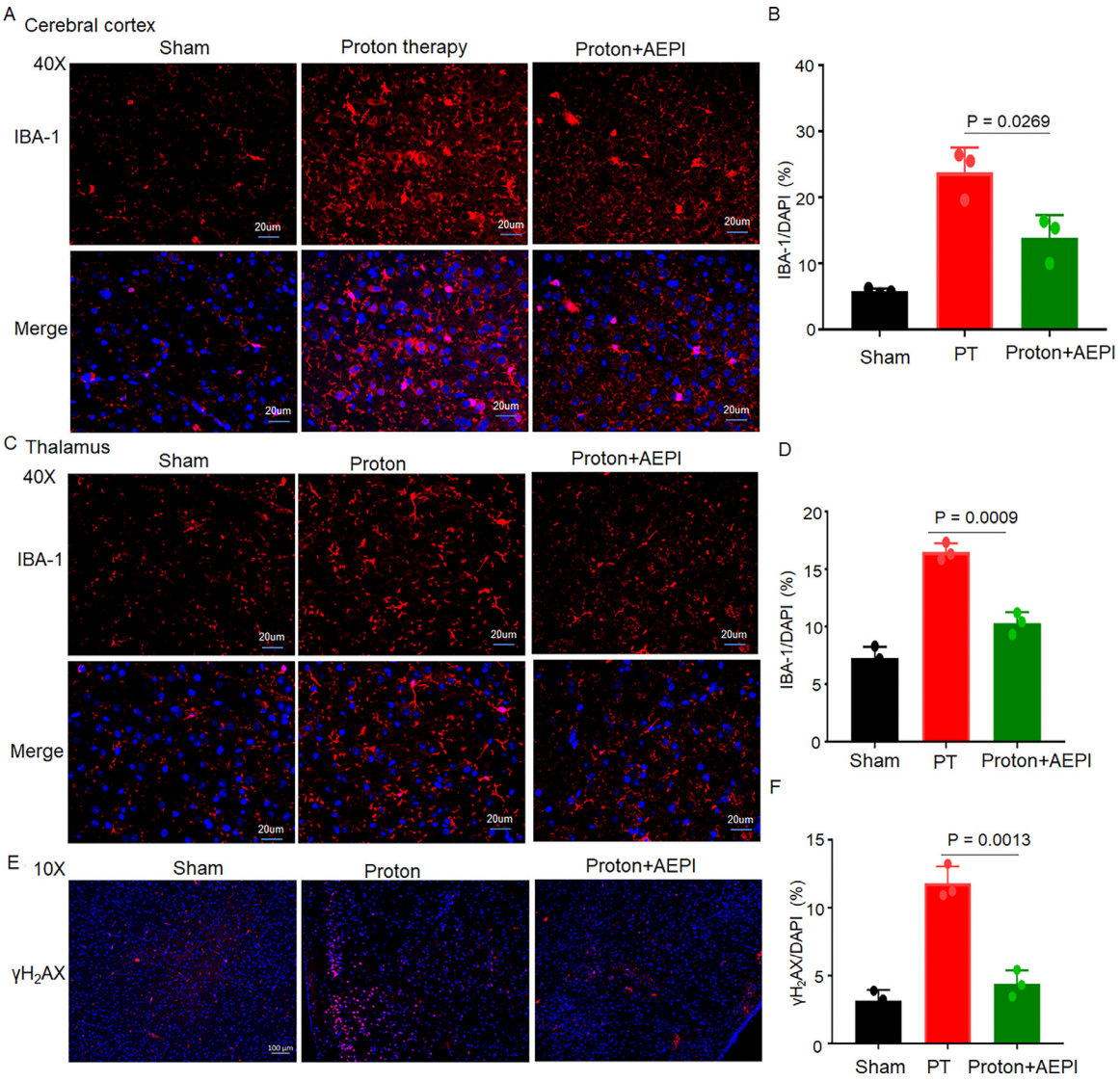

Figure 6 AEPI alleviated proton radiation-induced glial activation. (A, B) Representative fluorescence images of IBA1 immunostaining in a brain slice from the mouse cerebral cortex after different treatments. Scale bar: 20 μm. (C, D) Representative fluorescence images of IBA1 immunostaining in a brain slice from the mouse thalamus after different treatments. Scale bar: 20 μm. (E, F) Representative fluorescence images of γ-H2AX immunostaining in a brain slice from the mouse cortex after different treatments. Scale bar: 100 μm. Data are presented as mean ± SD from 3 independent experiments.
Abbreviations: AEPI = asparagine endopeptidase inhibitor; PT = proton therapy.

at several proton centers to reduce necrosis and other toxicities, but it does not fully address important biological concerns, such as linear energy transfer and RBE optimization.[19,20] More precise and thorough biological investigations are required to effectively address and prevent clinical damage as early as possible. Hence, we conducted this study to clarify the relative biological mechanism of the distal edge effect. Neuronal injuries appear to be partly mediated by activated microglia, and microglial activation inhibitors can alleviate the damaging effects of PT.

The RIBI model for studying the distal edge effect was established by delivering a proton beam to the left hemisphere, placing the right hemisphere in the distal (low-dose) or no-dose region. For comparison, photon beams were used horizontally and vertically to assess corresponding brain sections for neuronal and microglial changes. For vertical irradiation, lead blocking reduced the lateral penumbra and simulated the rapid drop at the proton distal edge. For horizontal irradiation directed from left to right, we used the same beam angle as in the proton model to study terminal photon injury. Notably, multiple sites in the cortex, thalamus, and frontal lobe, located farther from the distal edge of the BP (0.4633 ± 0.01856 cm), revealed signs of neuronal injury. As the proton beam moved linearly

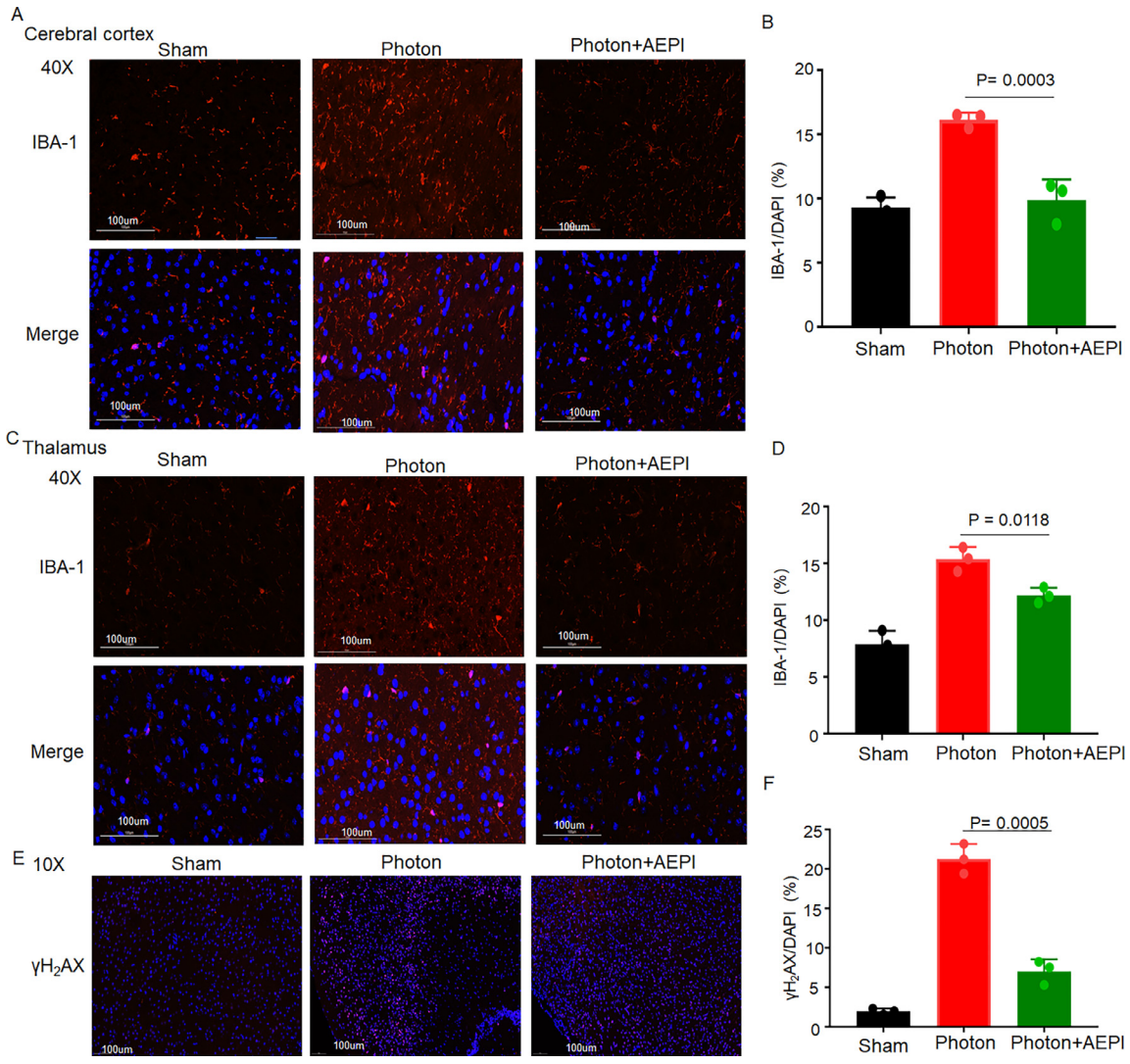

Figure 7 AEPI alleviated photon radiation-induced glial activation. (A, B) Representative fluorescence images of IBA1 staining in a brain slice from the mouse cerebral cortex after different treatments. Scale bar: 100 μm. (C, D) Representative fluorescence images of IBA1 immunostaining in a brain slice from the mouse thalamus after different treatments. Scale bar: 100 μm. (E, F) Representative fluorescence images of γ-H2AX immunostaining in a brain slice from the mouse cortex after different treatments. Scale bar: 100 μm. Data are presented as mean $\pm$ SD from 3 independent experiments.
Abbreviation: AEPI, asparagine endopeptidase inhibitor.

through the brain, multiple damage spots at significant distances in the low-dose zone or near the end of the range were observed that may be related to microglial activation. Many microglia with abnormal morphology accumulated at multiple injury sites, suggesting their involvement in the distal edge effect. Because of the high penetration of photons, horizontal irradiation resulted in increased neuronal injury and microglial activation, whereas vertical irradiated brain tissue did not show noticeable neuronal injury or microglial changes when compared with the area affected by the distal edge of the proton beam. This distal edge phenomenon of microglia activation and neuronal injury might be unique to protons. However, the specific mechanism by which these activated microglia injure neurons requires further exploration.

Irradiation can activate microglia via multiple pathways, including nuclear factor-κB, brain-derived neurotrophic factor, and high mobility group box 1 signaling.[21,22] Overactivated microglia can induce neuronal injury by releasing inflammatory cytokines, such as CCL2 and CCL8, and by recruiting $CD8^+$ T lymphocytes,[23] while also reducing the release of neurotrophic factors. Persistent microglial activation drives chronic neuroinflammation, potentially limiting brain neurogenesis and resulting in neurocognitive impairment in advanced stages of RIBI.[24] Meanwhile, microglia activated at the distal edge could exacerbate secondary neuronal

damage, which may be linked to long-term radiation brain damage reported in clinical patients.[6,7] Although Voshart et al[25] reported that protons lead to local molecular and morphologic changes in microglia without extending beyond the irradiated volume at 12 weeks postirradiation, our study was conducted 2 hours postirradiation and demonstrates that proton radiation activates microglia and causes distal neuronal injury in vivo. Because microglia undergo transient changes following radiation,[26] the distal edge microglia activation likely represents an early-phase alteration. Collectively, proton-induced brain damage may be reduced by optimizing irradiation regimens to consider linear energy transfer and by intervening early with protective medications targeting immune homeostasis.

Small-molecule proteasome inhibitors show considerable promise in disease treatment.[27] They block proteasome activity by forming reversible or irreversible covalent bonds with active sites of proteosomes. In the past 2 decades, 3 proteasome inhibitors (bortezomib, carfilzomib, and isazzomib) have been approved for clinical use.[28] AEP is activated in an acidic environment and is linked to the onset of certain nervous system disorders. We recently found that AEP expression was significantly elevated in the cortex and hippocampus of wild-type ($Lgmn^{+/+}$) mice after whole-brain irradiation. AEP causes neuroinflammation postirradiation by participating in antigen processing and presentation via microglia.[12] Here, an AEPI was shown to inhibit microglial activation and thus relieve neuronal damage in PT. Future research could explore balancing radioprotection and radio-efficacy.

In summary, our results showed that radiation injuries at the distal margin of the Bragg peak also occur in animal models. This notable injury appears to be influenced by activated microglia and was effectively prevented by AEPI.

Disclosures

The authors declare no conflict of interest.

Supplementary materials

Supplementary material associated with this article can be found in the online version at doi:10.1016/j.adro.2025.101764.

References

1. Yan S, Ngoma TA, Ngwa W, Bortfeld TR. Global democratisation of proton radiotherapy. *Lancet Oncol*. 2023;24:e245-e254. https://doi.org/10.1016/S1470-2045(23)00184-5.
2. Ioakeim-Ioannidou M, Goldberg S, Urell T, Tejada A, Nielsen GP, Hung YP, et al. Proton-based radiation therapy for skull base chondrosarcomas in children and adolescents: 40-year experience from the Massachusetts General Hospital. *Int J Radiat Oncol Biol Phys*. 2025;121:403-413.
3. Zhou Z, Guan B, Xia H, Zheng R, Xu B. Particle radiotherapy in the era of radioimmunotherapy. *Cancer Lett*. 2023;567:216268. https://doi.org/10.1016/j.canlet.2023.216268.
4. Chamseddine I, Shah K, Lee H, Ehret F, Schuemann J, Bertolet A, et al. Decoding patient heterogeneity influencing radiation-induced brain necrosis. *Clin Cancer Res*. 2024;30:4424-4433.
5. Johnson PB, Mamalui M, Brodin P, Janssens G. Secondary cancer risk in six anatomical sites when using PAT, IMPT, and VMAT/IMRT radiotherapy. *Radiother Oncol*. 2024;199:110421. https://doi.org/10.1016/j.radonc.2024.110421.
6. Harrabi SB, von Nettelbladt B, Gudden C, Adeberg S, Seidensaal K, Bauer J, et al. Radiation induced contrast enhancement after proton beam therapy in patients with low grade glioma - how safe are protons? *Radiother Oncol*. 2022;167:211-218.
7. Eulitz J, Troost EGC, Klünder L, Raschke F, Hahn C, Schulz E, et al. Increased relative biological effectiveness and periventricular radiosensitivity in proton therapy of glioma patients. *Radiother Oncol*. 2023;178:109422. https://doi.org/10.1016/j.radonc.2022.11.011.
8. Wang CC, McNamara AL, Shin J, Schuemann J, Grassberger C, Taghian AG, et al. End-of-range radiobiological effect on rib fractures in patients receiving proton therapy for breast cancer. *Int J Radiat Oncol Biol Phys*. 2020;107:449-454.
9. Liu Q, Huang Y, Duan M, Yang Q, Ren B, Tang F. Microglia as therapeutic target for radiation-induced brain injury. *Int J Mol Sci*. 2022;23:8286. https://doi.org/10.3390/ijms23158286.
10. Kim J, Sullivan O, Lee K, Jao J, Tamayo J, Madany AM, et al. Repeated LPS induces training and tolerance of microglial responses across brain regions. *J Neuroinflammation*. 2024;21:233. https://doi.org/10.1186/s12974-024-03198-1.
11. Wei W, Lattau SSJ, Xin W, Pan Y, Tatenhorst L, Zhang L, et al. Dynamic brain lipid profiles modulate microglial lipid droplet accumulation and inflammation under ischemic conditions in mice. *Adv Sci (Weinh)*. 2024;11:e2306863. https://doi.org/10.1002/advs.202306863.
12. Qiu O, Zhao J, Shi Z, Li H, Wang S, Liao K, et al. Asparagine endopeptidase deficiency mitigates radiation-induced brain injury by suppressing microglia-mediated neuronal senescence. *iScience*. 2024;27:109698. https://doi.org/10.1016/j.isci.2024.109698.
13. Qian Z, Li B, Meng X, Liao J, Wang G, Li Y, et al. Inhibition of asparagine endopeptidase (AEP) effectively treats sporadic Alzheimer's disease in mice. *Neuropsychopharmacology*. 2024;49:620-630.
14. Wu Z, Zhu R, Yu Y, Wang J, Hu X, Xu W, et al. Spinal cord injury-activated C/EBPβ-AEP axis mediates cognitive impairment through APP C586/Tau N368 fragments spreading. *Prog Neurobiol*. 2023;227:102467. https://doi.org/10.1016/j.pneurobio.2023.102467.
15. Krummenacher D, He W, Kuhn B, Schnider C, Beurier A, Brom V, et al. Discovery of orally available and brain penetrant AEP inhibitors. *J Med Chem*. 2023;66:17026-17043.
16. Fowler JF. The linear-quadratic formula and progress in fractionated radiotherapy. *Br J Radiol*. 1989;62:679-694.
17. Dokic I, Meister S, Bojcevski J, Tessonnier T, Walsh D, Knoll M, et al. Neuroprotective effects of ultra-high dose rate FLASH Bragg peak proton irradiation. *Int J Radiat Oncol Biol Phys*. 2022;113:614-623.
18. Missiaggia M, Cartechini G, Tommasino F, Scifoni E, La Tessa C. Investigation of in-field and out-of-field radiation quality with microdosimetry and its impact on relative biological effectiveness in proton therapy. *Int J Radiat Oncol Biol Phys*. 2023;115:1269-1282.
19. Giantsoudi D, Adams J, MacDonald SM, Paganetti H. Proton treatment techniques for posterior fossa tumors: Consequences for linear

energy transfer and dose-volume parameters for the brainstem and organs at risk. *Int J Radiat Oncol Biol Phys*. 2017;97:401-410.
20. Luo L, Lin S, Hu G, Wu J, Hu Y, Nong F, et al. Molecular mechanism of Rolupram reducing neuroinflammation in noise induced tinnitus mice through TLR4/NF kB/NLRP3 protein/caspase-1/IL-1 β signaling pathway. *Int J Biol Macromol*. 2024;278:134987. https://doi.org/10.1016/j.ijbiomac.2024.134987.
21. Wang Y, Tian J, Liu D, Li T, Mao Y, Zhu C. Microglia in radiation-induced brain injury: Cellular and molecular mechanisms and therapeutic potential. *CNS Neurosci Ther*. 2024;30:e14794. https://doi.org/10.1111/cns.14794.
22. Xu B, Yin M, Yang Y, Zou Y, Liu W, Qiao L, et al. Transplantation of neural stem progenitor cells from different sources for severe spinal cord injury repair in rat. *Bioact Mater*. 2023;23:300-313.
23. Shi Z, Yu P, Lin WJ, Chen S, Hu X, Chen S, et al. Microglia drive transient insult-induced brain injury by chemotactic recruitment of $CD8^+$ T lymphocytes. *Neuron*. 2023;111:696-710.e9.
24. Summers RA, Fagiani F, Rowitch DH, Absinta M, Reich DS. Novel human iPSC models of neuroinflammation in neurodegenerative disease and regenerative medicine. *Trends Immunol*. 2024;45:799-813.
25. Voshart DC, Klaver M, Jiang Y, van Weering HRJ, van Buuren-Broek F, van der Linden GP, et al. Proton therapy induces a local microglial neuroimmune response. *Radiother Oncol*. 2024;193:110117.
26. Osman AM, Sun Y, Burns TC, He L, Kee N, Oliva-Vilarnau N, et al. Radiation triggers a dynamic sequence of transient microglial alterations in juvenile brain. *Cell Rep*. 2020;31:107699. https://doi.org/10.1016/j.celrep.2020.107699.
27. Devasia AJ, Chari A, Lancman G. Bispecific antibodies in the treatment of multiple myeloma. *Blood Cancer J*. 2024;14:158. https://doi.org/10.1038/s41408-024-01139-y.
28. Tyrna P, Procyk G, Szeleszczuk Ł, Młynarczuk-Biały I. Different strategies to overcome resistance to proteasome inhibitors-a summary 20 years after their introduction. *Int J Mol Sci*. 2024;25:8949. https://doi.org/10.3390/ijms25168949.